

RESEARCH

Open Access



Construction and validation of a novel Ferroptosis-related gene signature predictive model in rectal Cancer

Wei-Kun Shi¹, Yu-Xin Liu¹, Xiao-Yuan Qiu¹, Jing-Ya Zhou^{2,3}, Jiao-Lin Zhou¹ and Guo-Le Lin^{1*}

Abstract

Background: Rectal cancer (RC) is one of the most common malignant tumors. Ferroptosis is an iron-dependent form of cell death, which plays an important role in various cancers. However, the correlation between ferroptosis-related genes (FRGs) and prognosis in RC remains unclear.

Methods: Gene expression data from The Cancer Genome Atlas Rectum adenocarcinoma (TCGA-READ) and GSE87211 were downloaded. Clustering and functional enrichment were evaluated. A FRGs risk score was established based on the univariate Cox analysis and the Least absolute shrinkage and selection operator (LASSO) analysis. K-M analysis and ROC analysis were conducted to determine prognostic values. qRT-PCR was performed to validate levels of mRNA expression. Multivariate Cox analysis was used to build a prognostic prediction model based on the risk score.

Results: Based on FRGs, RC patients were grouped into two clusters. In the functional enrichment of differentially expressed genes between the two clusters, immune-related pathways dominated. A novel FRGs signature with 14 genes related to the overall survival (OS) of RC was established. qRT-PCR of the 14 genes identified TP63, ISCU, PLIN4, MAP3K5, OXSR, FANCD2 and ATM were overexpressed in RC tissue; HSPB1, MAPK1, ABCC1, PANX1, MAPK9 and ATG7 were underexpressed; TUBE1 had no difference. The high-risk group had a significantly lower OS than the low-risk group ($P < 0.001$), and ROC curve analysis confirmed the signature's predictive capacity. Multivariate analysis demonstrated that the risk score and age were independent prognostic factors.

Conclusion: A novel FRGs model can be used to predict the prognosis in RC, as well as to guide individual treatment.

Keywords: Rectal cancer, Prognosis, Ferroptosis-related genes, Risk score

Introduction

Colorectal cancer (CRC) is the third most prevalent cancer worldwide, and rectal cancer (RC) accounts for approximately 40% of all CRCs [1]. RC is the eighth

leading cause of cancer-related mortality globally, with about 339,022 deaths in 2020 [2].

Due to the popularization of digestive endoscopy and the development of MRI, endoscopic ultrasound and other technologies, early diagnosis of RC has been greatly improved [3, 4], and the method of treatment has also been developed from a single TME (total mesorectal excision) radical operation to a multidisciplinary combined treatment modality including neoadjuvant chemoradiotherapy (nCRT) along with organ-sparing surgery [5]. However, the prognosis of RC remains unsatisfactory.

*Correspondence: linguole@126.com

¹ Department of General Surgery, Peking Union Medical College Hospital, Peking Union Medical College and Chinese Academy of Medical Sciences, Shuaifuyuan 1, Beijing 100730, China
Full list of author information is available at the end of the article



Despite nCRT combined with radical surgery and adjuvant chemotherapy, the long-term distant metastasis rate after surgery can still reach 30% [6], and the 10-year survival rate may be below 50% [7].

Some molecular biological diagnostic techniques have been applied to diagnose, treat and predict the prognosis of RC, such as monitoring circulating tumor DNA (ctDNA) expression levels to predict the prognosis [8], detecting UGT1A1 gene polymorphisms to predict the chemotherapy sensitivity [9], detecting microsatellite instability to predict the efficacy of immune checkpoint inhibitors (ICI) [10]. With the ultimate goal of improving the patient's prognosis, these technologies can make the treatment of RC more accurate. Hence, an in-depth discussion of the diagnosis and treatment of RC at the molecular level is the current research hotspot and the direction of future development. We need to further explore molecular targets for the diagnosis and treatment of RC. In addition, we need to provide novel methods for the diagnosis, treatment, and prognostic prediction of RC patients through various mechanisms.

Ferroptosis is an iron-dependent programmed cell death pattern characterized by the accumulation of lipid peroxides, proposed by Stockwell et al. in 2012 [11]. The core molecular mechanism of ferroptosis includes regulating the balance between oxidative damage and antioxidant defense, which requires the precise regulation of ferroptosis-related genes (FRGs) and their expression products, and this balancing process also greatly affects the occurrence and development of tumor cells [12]. Numerous studies have explored the relationship between ferroptosis and malignant tumors at the genetic level, such as trying to treat renal clear cell carcinoma by glutathione peroxidase 4 (GPX4)-dependent ferroptosis [13], inhibiting ALOX5 may promote ferroptosis in pancreatic ductal adenocarcinoma [14], SLC7A11-mediated cystine uptake inhibits ferroptosis in breast cancer cells [15] etc. Based on a large number of studies, some researchers have summarized the related literature on ferroptosis, and classified the genes involved into a database [16]. This may provide better support for our research on the mechanism of ferroptosis.

The clinical application of ferroptosis focuses on targeting the expression of some FRGs to specifically induce ferroptosis in tumor cells, thus obtaining anti-cancer effects [17, 18]. In order to obtain detailed information about a target, it is usually necessary to perform bioinformatics analysis to determine whether tumor tissue differs from normal or paracancerous tissues. In CRC, there are some studies discussing the role of FRGs, for example, activation of ATF3 may promote ferroptosis by inhibiting the Xc⁻ system [19]; CDKN2A sensitizes cancer cells to ferroptosis by downregulating

SLC7A11 [20]. Some studies also use a set of FRGs to develop a risk model for predicting the prognosis of CRC [21, 22]. However, such studies on ferroptosis and RC alone are lacking.

It is necessary for us to analyze FRGs in RC, find ferroptosis-related markers, and evaluate their prognostic value, so as to provide reference for further basic research and clinical translation.

Materials and methods

Data source

The Cancer Genome Atlas (TCGA) (<https://portal.gdc.cancer.gov/>) contains 167 rectum adenocarcinoma (READ) tumor samples and GSE87211 acquired from Gene Expression Omnibus (GEO) (<https://www.ncbi.nlm.nih.gov/geo/>) which include 196 RC patients were used as training set and external validation sets, respectively. We obtained human FRGs from the FerrDB database (<http://www.datjar.com:40013/bt2104/>). The Human Protein Atlas (HPA) (<https://www.proteinatlas.org/about/download>) was used to verify the immunohistochemical (IHC) staining of genes.

Clustering and identification of differentially expressed genes (DEGs)

The ConsensusClusterPlus R package [23] was used to perform unsupervised clustering and divide the RC into two clusters according to the FRGs. This method is based on an algorithm called consensus clustering, which can provide quantitative evidence for determining the number of potential clusters within the RNA-seq data. The t-distributed stochastic neighbor embedding (t-SNE) analysis was applied based on FRGs to visualize the data in two dimensions with the Rtsne and ggplot2 packages [24]. Then, the limma R package [25] was used to analyze the ferroptosis-related DEGs (FRDEGs) between these two groups. FRDEGs were identified based on *P* value < 0.05 and the absolute value of Fold Change > 1 ($|\text{Log}_2\text{fold change}| > 1$). Volcano plots and a Venn diagram were drawn with the ggplot2 R package. The heat map was generated by the pheatmap R package.

Gene ontology (GO) and Kyoto encyclopedia of genes and genomes (KEGG) analysis

GO analysis, including biological process (BP), cellular composition (CC) and molecular function (MF), was performed for FRDEGs characteristics using the clusterProfiler R package [26]. We also used this package to analyze the functional enrichment of the FRDEGs in KEGG pathways [27].

Establishment and validation of the risk score based on the FRGs

The univariate Cox regression analysis was performed to determine the FRGs with the prognostic value, and the cutoff p -value was set at 0.05. Then, least absolute shrinkage and selection operator (LASSO) regression was performed to further screen relevant key genes. Ten-fold cross-validation was used to select the most suitable model parameters λ . Next, we used these key genes to calculate a risk score, which was obtained using the formula: risk score = $(\beta_A \times \text{Gene A expression}) + (\beta_B \times \text{Gene B expression}) \dots + (\beta_N \times \text{Gene N expression})$. According to the median risk score, RC patients were divided into two groups: the low-risk group and the high-risk group. The survival differences between the low- and high-risk groups were compared through Kaplan-Meier (K-M) analysis. In addition, we also performed receiver operating characteristic (ROC) analysis to assess the survival predictive ability of this risk score. The GEO dataset was used as a validation group to verify the above outcomes.

Quantitative real-time PCR (qRT-PCR)

qRT-PCR was performed on 10 pairs of RC tissues and adjacent normal tissues to validate the mRNA expression levels of the 14 signature genes. Consent forms were obtained from each patient for the collection and analysis of tissue samples. The study was approved by the Peking Union Medical College Hospital ethics review boards. We immediately froze and stored the tissues in liquid nitrogen after extracting them. Total RNA was extracted from the sample tissues via Trizol lysate (Thermo Fisher Scientific), followed by reverse transcription to cDNA. qRT-PCR was carried out using the CFX96 system (BIO-RAD CFX96; BIO-RAD Laboratories, Inc., Hercules, CA, USA). GAPDH served as an internal control. Relative expression levels were quantified by the Ct ($2^{-\Delta\Delta C_t}$) method, and the mean value was used as the final experimental result for replicated wells. All procedures were carried out in accordance with the manufacturer's instructions.

Gene set enrichment analysis (GSEA)

To explore the different KEGG pathways between high- and low-risk groups, GSEA was conducted with the Molecular Signatures Database (MSigDB). Pathways with an adjusted $P < 0.05$ were identified as significant enrichment pathways in various risk groups.

Evaluation of immune microenvironment characteristics, immune checkpoint related characteristics and chemotherapy drugs' sensitivity.

xCELL [28] algorithm was used to estimate the abundance scores of 64 immune cells per sample. Tumor

mutation burden (TMB) was calculated according to the mutation information from TCGA READ cohort. The TMB estimate for each sample is equal to the total mutation frequency/38, since 38Mb is routinely taken based on the length of the human exon. To predict the effect of immune checkpoint blockade therapy, the expression of 34 potential immune checkpoint genes was analyzed. Furthermore, the Tumor Immune Dysfunction and Exclusion (TIDE) (<http://tide.dfci.harvard.edu/>) algorithm was used to estimate the ICIs response of RC patients from TCGA cohort [29]. The pRRophetic R package [30] was used to evaluate the sensitivity of chemotherapy drugs. Compare the above characteristics of high- and low-risk groups for diagrams.

Establishment of the prognostic model

Univariate and multivariate Cox regression analyses were performed to establish the prognostic model based on the risk score and other clinical/pathological characteristics (age and TNM stage) of the patients. We constructed a nomogram to predict the overall survival (OS) of RC patients in 1-, 3- and 5-year according to the prognostic model. Then, we used the median total points for each patient based on this nomogram, to divide patients into high-risk and low-risk groups. The K-M curve was plotted and ROC analysis was carried out at 1-, 3- and 5-year of survival. Next, calibration curves were used to estimate whether the predicted survival results of the nomogram (1-, 3- and 5-year survival) were close to the actual results.

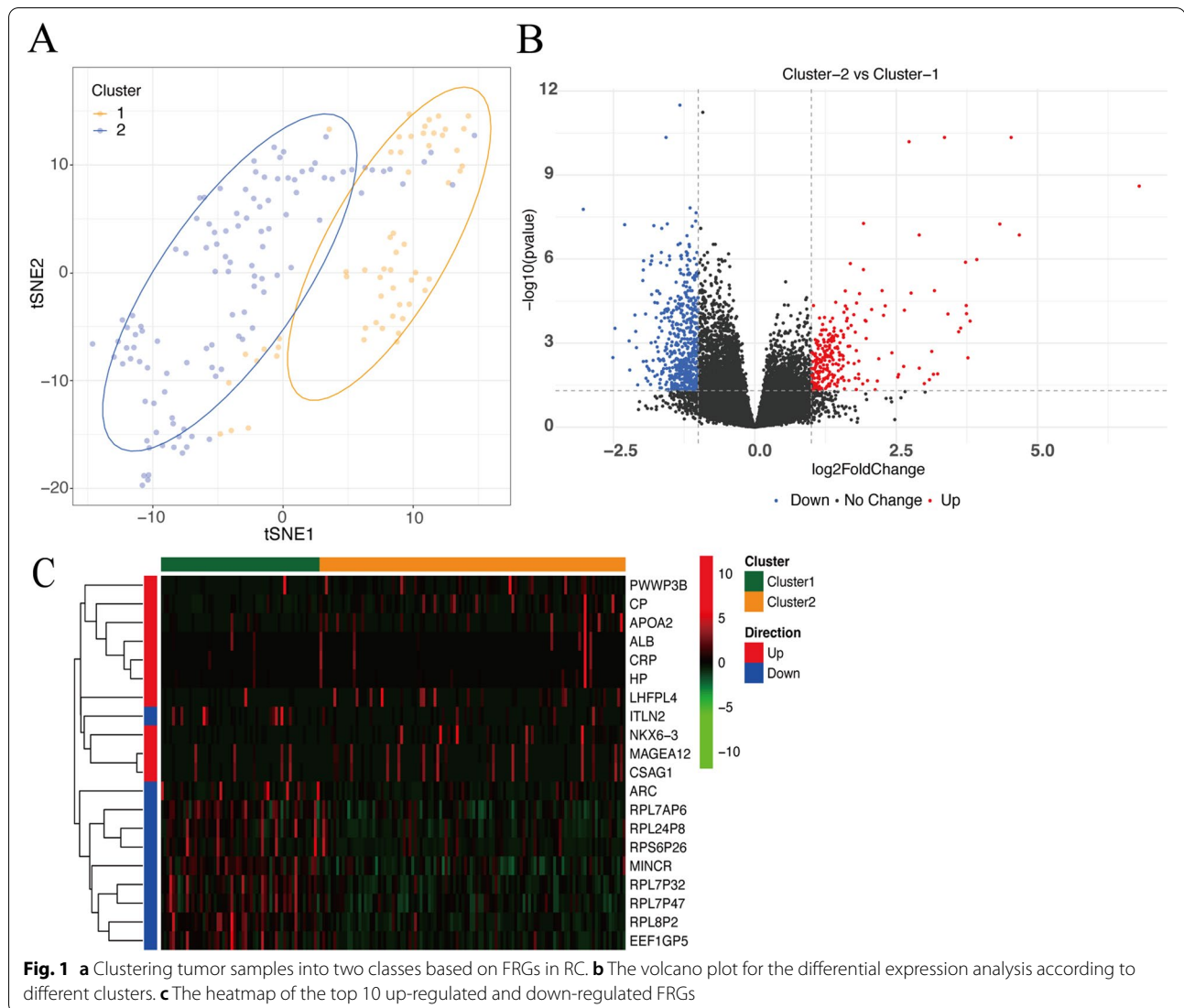
Statistical analysis

All analyses were performed using R version 4.1.3 (<https://www.r-project.org/>) and its appropriate packages. Univariate, LASSO and multivariate Cox regression analyses were conducted to build models. Log-rank test was used in the K-M analysis. Two groups were adjusted by the Wilcoxon test and the p -value was corrected by Benjamini and Hochberg (BH) test. Two-sided $P < 0.05$ indicated statistical significance.

Results

FRGs were clustered in patients with RC, followed by the identification of DEGs and functional enrichment analysis.

Cluster analysis of TCGA READ gene expression data using FRGs can divide RC patients into two clusters (Cluster 1 and Cluster 2). Visualization of the two groups after dimensionality reduction was shown in Fig. 1(a). We conducted the subsequent analysis based on two clusters, and also provided consensus matrix heatmaps of 3 to 9 clusters for readers' reference (Supplementary Fig. 1). We obtained 822 DEGs, 263 genes were up-regulated and



559 were down-regulated (Fig. 1(b)). The heatmap of the top 10 up-regulated and top 10 down-regulated genes was shown in Fig. 1(c).

The results of the GO enrichment analysis were presented in Fig. 2(a-c), which showed the enrichment of the 20 most significant pathways (ranked according to the adjusted p -value) in BP, CC and MF respectively. Differential genes were enriched in immune-related pathways in each facet, and were additionally associated with phagocytosis, transmembrane transport, GABA receptors, ion channels etc. The result of the KEGG enrichment analysis was shown in Fig. 3. As with the GO enrichment analysis, differential gene expression was associated with immune pathways using KEGG enrichment analysis. This analysis also found associations with PPAR, retinol metabolism, P450 enzymes and drug metabolism, and the nervous system.

Establishment of a risk score

Using univariate Cox regression analysis with FRGs in the training group, 16 genes were correlated with the OS of RC patients ($P < 0.05$) (Fig. 4). To prevent model overfitting, 14 genes (TP63, ISCU, HSPB1, PLIN4, MAPK1, ABCC1, MAP3K5, OXSR1, PANX1, MAPK9, FANCD2, ATM, TUBE1 and ATG7) were selected by LASSO regression (Figs. 5(a) and 5(b)). When the minimum λ value was 0.002521672, the following risk score formula was obtained: Riskscore = (5.076640326) * TP63 + (2.175090008) * ISCU + (0.018180284) * HSPB1 + (0.593316672) * PLIN4 + (0.155545632) * MAPK1 + (0.136338804) * ABCC1 - (0.271718945) * MAP3K5 + (0.670705631) * OXSR1 - (0.266461901) * PANX1 - (0.928347939) * MAPK9 - (0.230410588) * FANCD2 - (1.069047524) * ATM - (1.559344596) * TUBE1 - (1.51520076) * ATG7. Based on the median

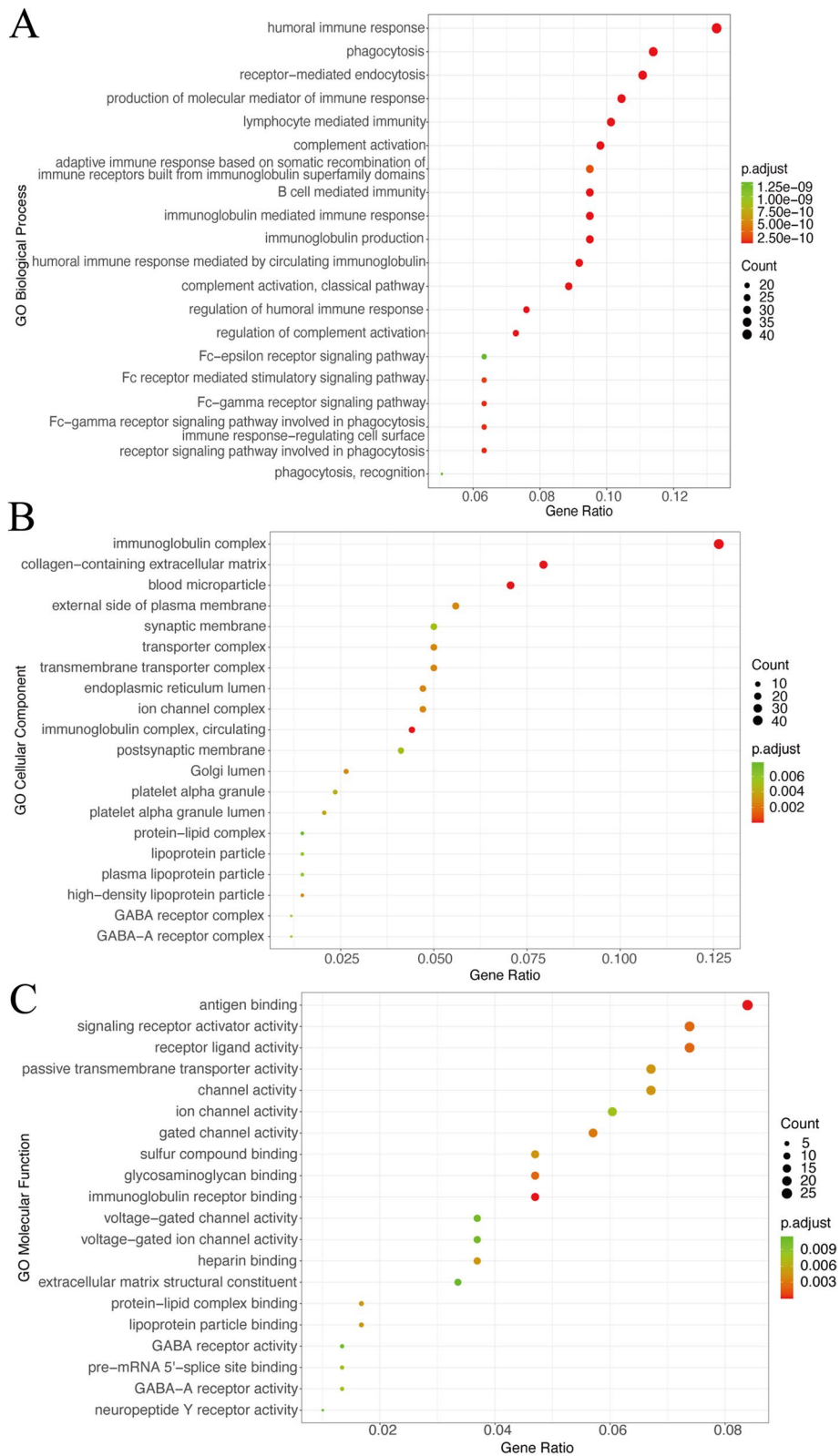
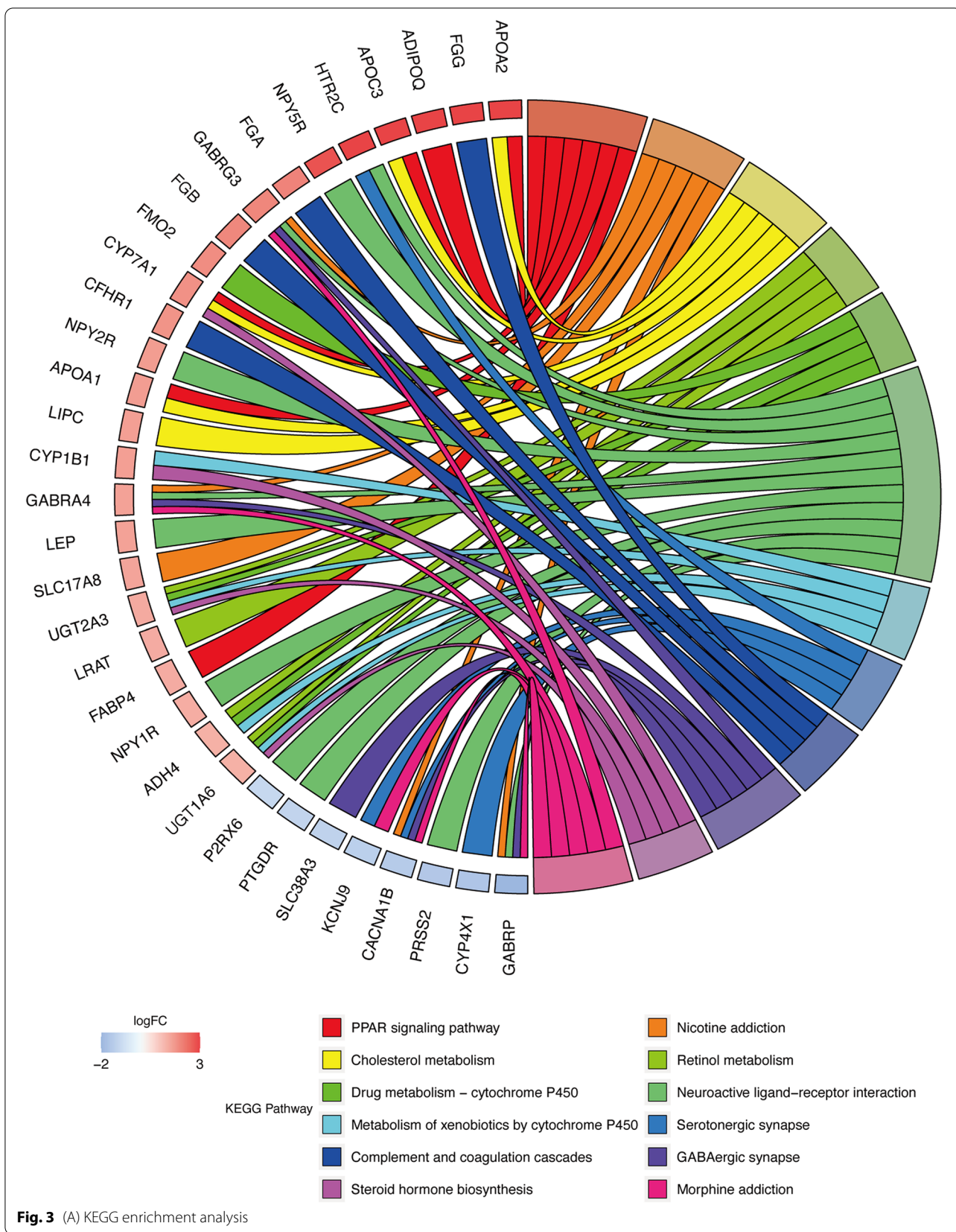


Fig. 2 a-c BP, CC and MF of GO analysis



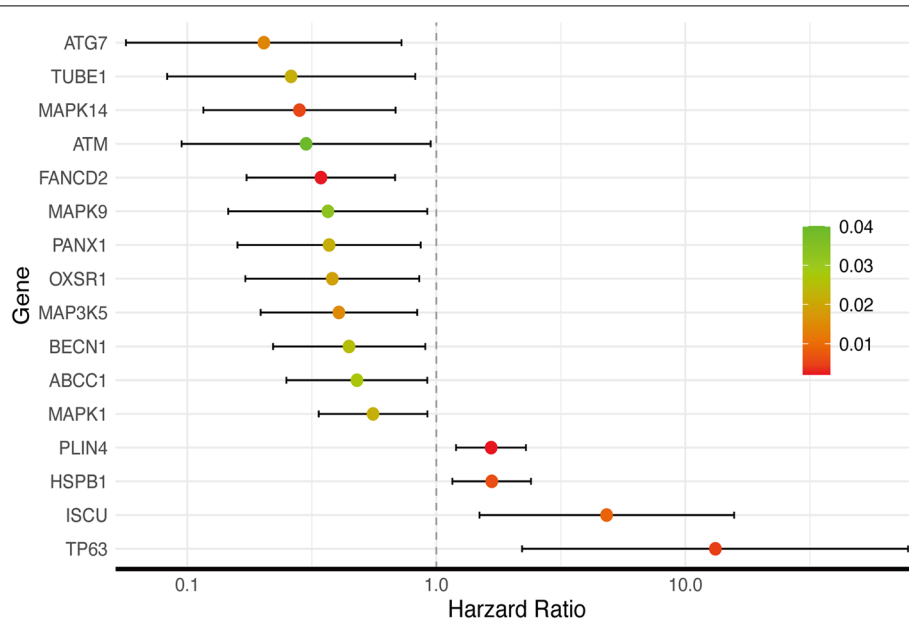


Fig. 4 The univariate Cox regression analysis of the training group show 16 FRGs were correlated with OS

of the risk score, we separated the cases into two groups: high-risk and low-risk groups (Fig. 5(c)). The risk distribution plot revealed that the high-risk group had significantly higher mortality and shorter OS than the low-risk group (Fig. 5(d)). The K-M curve indicated that the high-risk group had a significantly worse OS ($P < 0.001$) with a hazard ratio (HR) of 8.36 (95%CI 3.95–17.7) (Fig. 5(e)). The area under curves (AUCs) of 1-, 3-, and 5-year OS were 0.83, 0.813 and 0.959 according to ROC curves (Fig. 5(f)).

Validation of the risk score using the GEO cohort

We then evaluated the prognostic efficiency of the risk model by analyzing the data of RC from the GEO dataset (GSE87211). The distribution of risk scores and survival status in the dataset is presented in Fig. 6(a) and 6(b). Likewise, as the risk score increased, the number of deaths also increased. Similar to the results from the TCGA cohort, the high-risk group had a significantly poorer OS in the GEO dataset ($P = 0.0381$) with a HR of 2.26 (95%CI 1.08–4.74) (Fig. 6(c)). The AUCs for 1-, 3- and 5-year OS were 0.623, 0.717 and 0.673, respectively, in the GEO dataset (Fig. 6(d)).

IHC differences using the HPA database

To further confirm the importance of the 14 FRGs in the risk score, HPA database was used to compare their protein expression in non-cancerous and RC tissues. According to Fig. 7, only ATM was highly expressed in RC tissue

as compared to normal rectal tissue. In contrast, HSPB1, MAPK1, ABCC1, PANX1, MAPK9 and ATG7 were downregulated in RC. The protein levels of TP63, ISCU, PLIN4, MAP3K5, OXSR1, FANCD2 and TUBE1 had no significant changes between RC and normal rectal tissue.

qRT-PCR

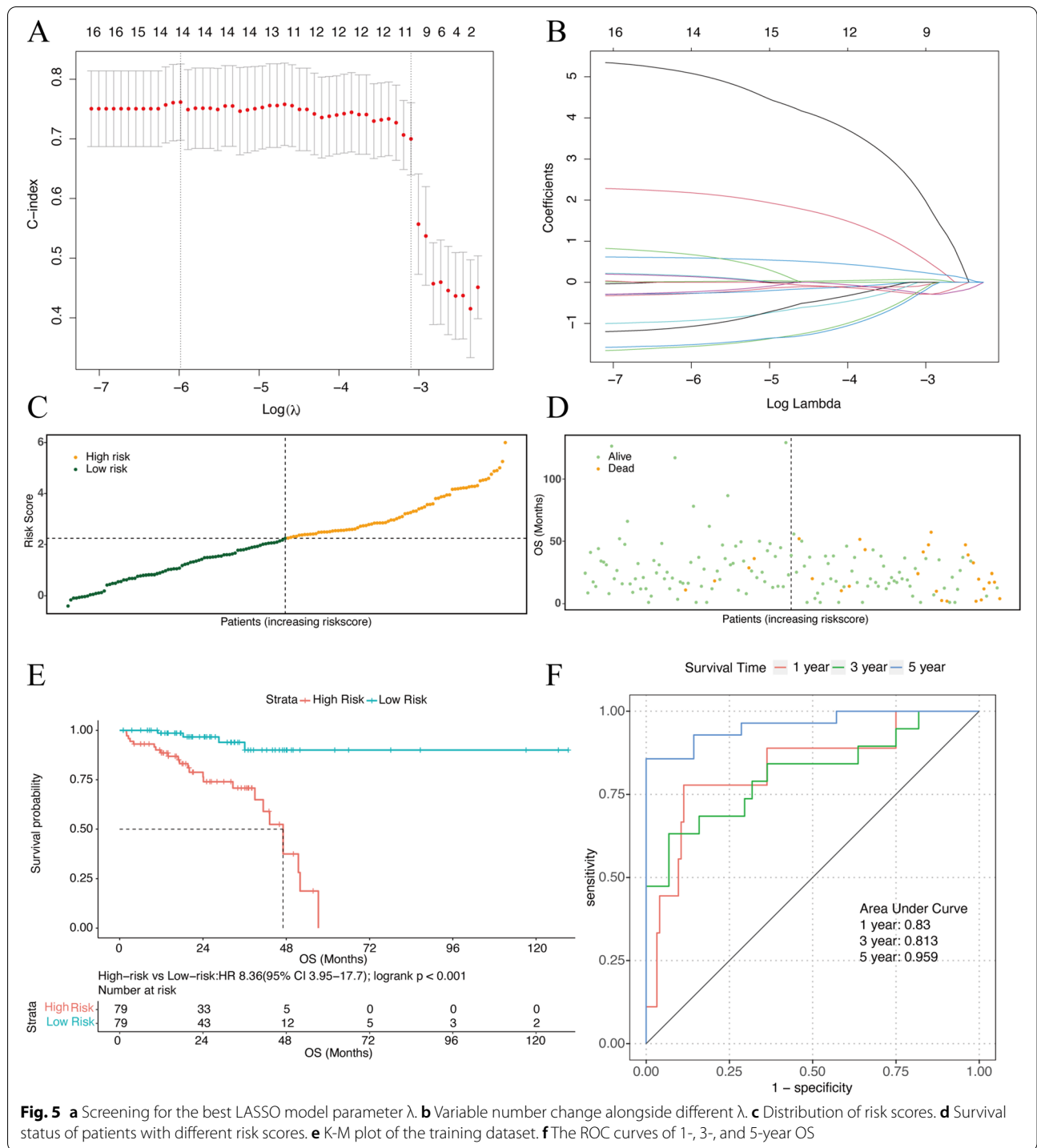
In RC tissue, the expression of TP63, ISCU, PLIN4, MAP3K5, OXSR, FANCD2 and ATM was significantly higher than that of normal tissue. In contrast, the expression of HSPB1, MAPK1, ABCC1, PANX1, MAPK9 and ATG7 was significantly lower than that of normal tissue. There was no significant difference in the expression of TUBE1. (Fig. 8).

GSEA

The pathways of ribosomes, oxidative phosphorylation, and arachidonic acid metabolism were mainly enriched in high-risk groups. In contrast, the pathways of DNA replication, homologous recombination, RNA degradation, cell cycle and spliceosome were mainly enriched in the low-risk group (Fig. 9).

Prognostic FRDEGs had minor effects on the immune microenvironment of RC

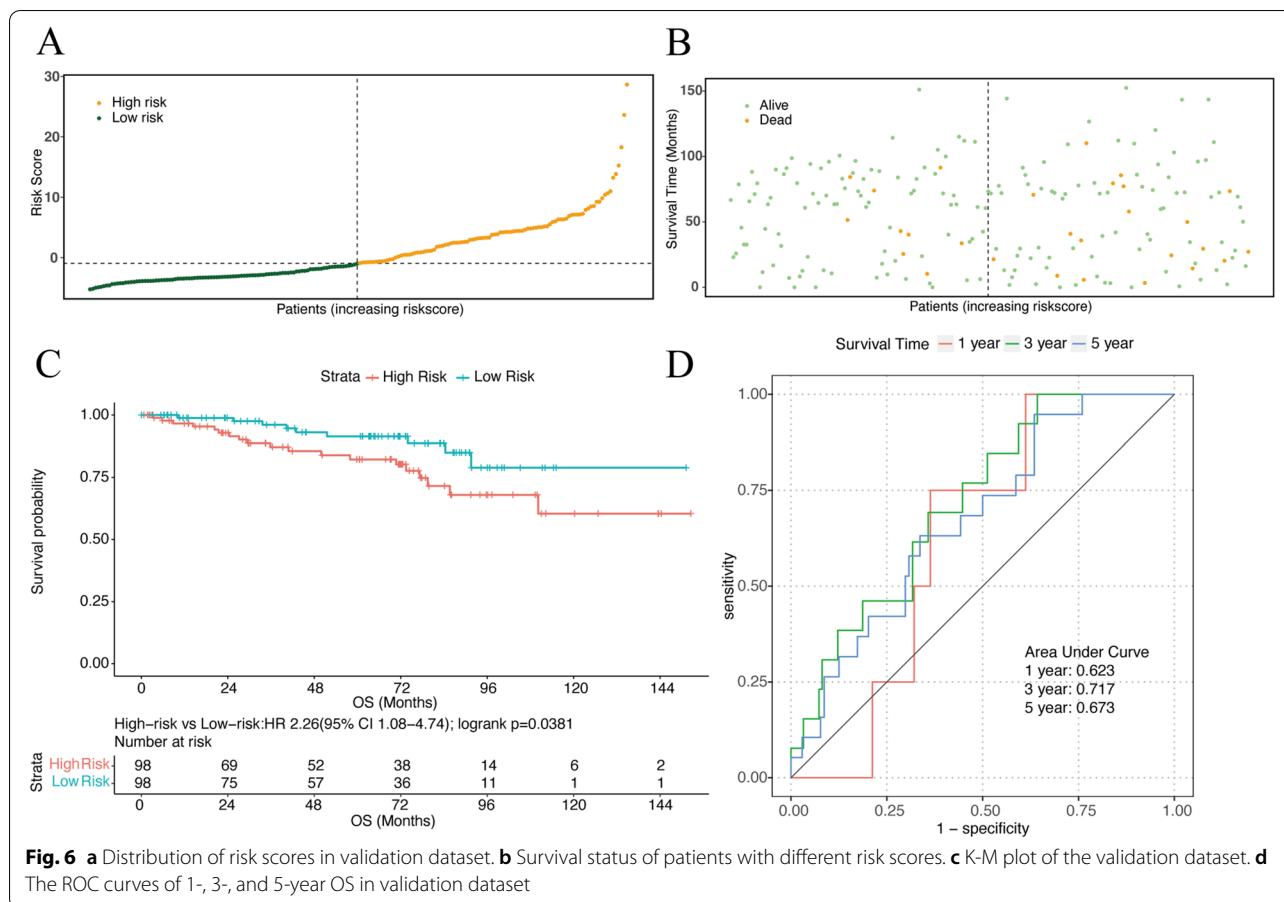
We compared immune infiltration by xCELL between patients in the low- and high-risk groups and observed that the infiltration levels of CD4⁺ Tem, CD8⁺ naive T-cells, mast cells, monocytes, NK cells, Tgd cells, Th2 cells were significantly different (Fig. 10(a)). There was no



statistical difference in TMB between the high- and low-risk groups (Fig. 10(b)). The TIDE analysis data showed that the high-risk group had a statistically larger dysfunction score than the low-risk score, while the exclusion score had no difference (Fig. 10(c) and (d)). In the evaluation of 34 immune checkpoint gene expressions, only CD155 was significantly different (Fig. 10(e)).

Analysis of the relationship between the risk model and chemotherapy

The results showed that there were some chemotherapeutic drugs with significantly different IC50s between the high- and low-risk groups, among which the more sensitive drugs in the high-risk group were: AS605240, CI-1040, QS11, OSI-027, MK-2206, Cetuximab and MP470 (Fig. 11).



Construction of the nomogram

Based on the univariate and multivariate Cox regression analysis of the risk score and clinical traits (age and TNM stage) (Fig. 12(a) and (b)) in the training cohort, we built a prognostic nomogram to predict 1, 3 and 5-year OS probabilities of RC patients (Fig. 12(c)). The calibration curves demonstrated that the model’s predictions of 1, 3 and 5-year OS probabilities were favorably consistent with the ideal predictions (Fig. 12(d-f)).

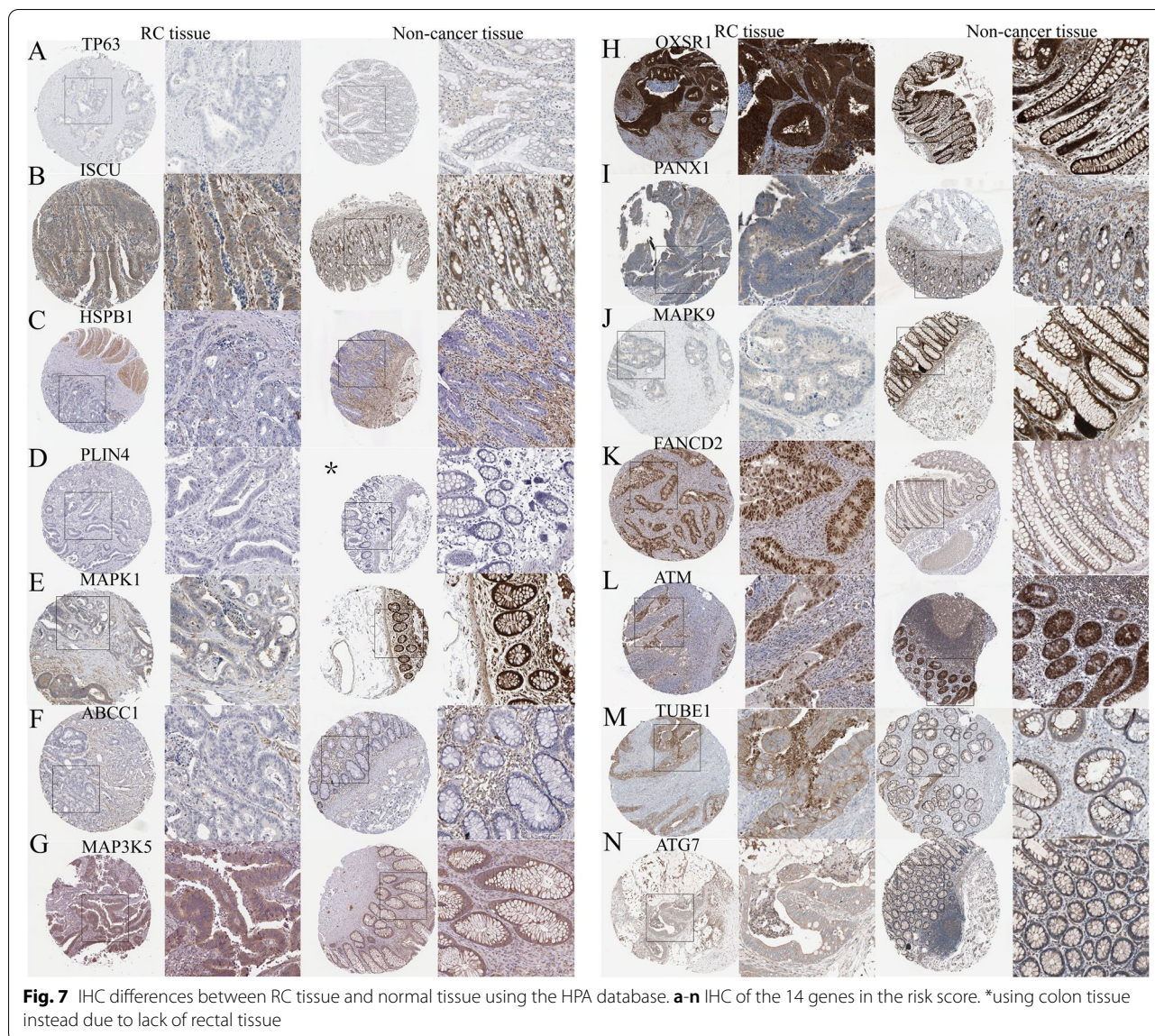
Discussion

RC is a dangerous malignant tumor that threatens human health. At present, the efficacy of comprehensive treatment needs to be improved. Many molecular mechanisms are still being explored, and many reasons for the occurrence and development of RC are still unclear. Ferroptosis is an iron-dependent form of cell death. In the field of malignant tumors, people hope to inhibit tumor development by promoting ferroptosis in tumor tissue, and providing new targets and a pharmacological basis for tumor therapy.

In this study, the risk score of FRGs in RC was established by analyzing the transcriptome, clinical information, and survival information of TCGA READ. A risk

prediction model was built on the basis of the risk score, combined with multivariate Cox analysis. The model can effectively predict the 1-, 3- and 5-year OS of RC, providing a potentially useful tool for clinical practice and further mechanism research.

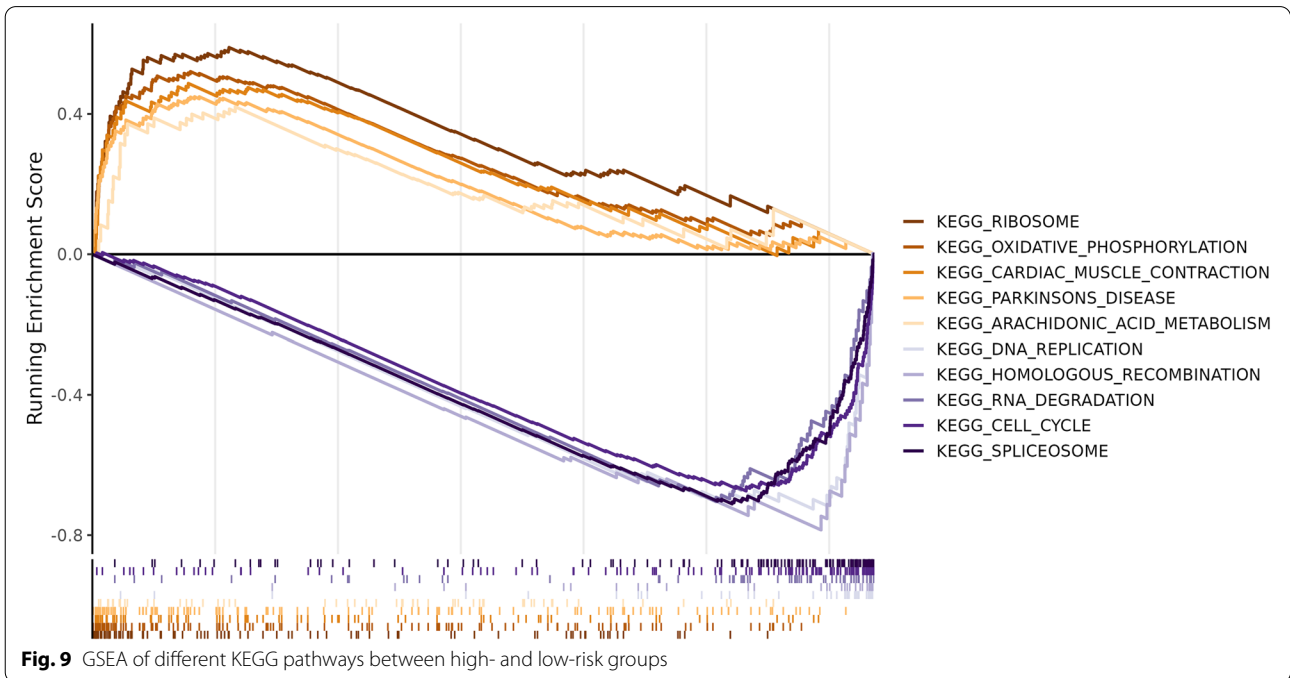
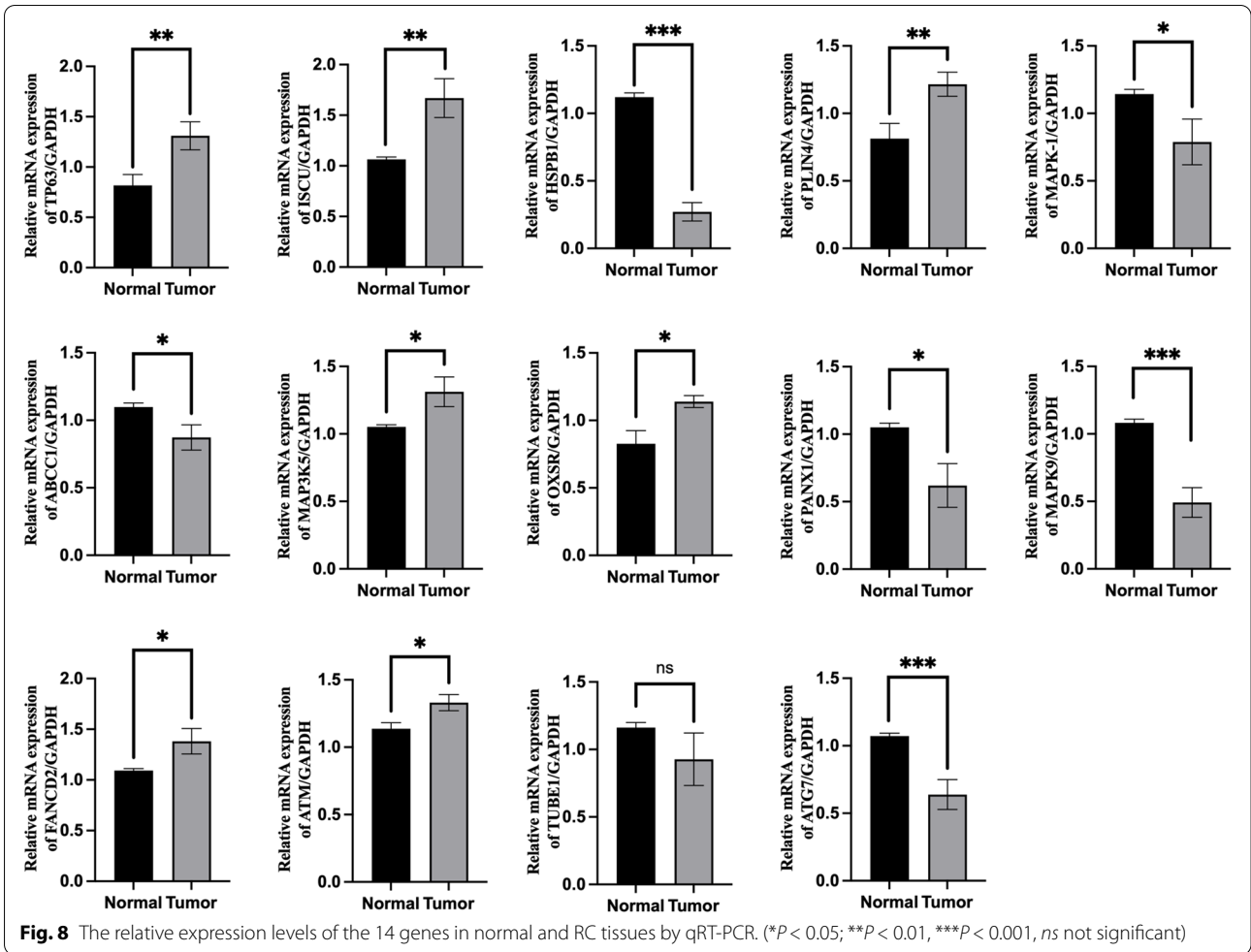
First, we performed a cluster analysis on TCGA READ samples from the perspective of FRGs. The clustering results were divided into two categories, meaning that the RCs were divided into two different types of ferroptosis gene expression patterns. We use GO enrichment analysis and find that these FRDEGs are mainly enriched in immunity in BP, CC and ME. This suggests that the differences in gene expression of ferroptosis in RC patients are closely related to immune responses. Many studies have shown that ferroptosis is closely associated with the tumor immune microenvironment [31]. The study by Fushun et al. found that BEBT-908-induced ferroptosis results in upregulation of MHC I and activation of endogenous IFN γ signaling in tumor cells, thereby improving cancer immunotherapy [32]. There will be further studies on ferroptosis and cancers, including RC, from the perspective of immunotherapy, in an effort to benefit patients.



To further investigate FRGs affecting RC, univariate Cox regression was applied to screen genes significantly associated with OS. Then, 14 genes were identified using LASSO regression to establish a risk score. We divided patients into the high- and low-risk groups by the risk score, and survival analysis indicated that the prognosis of the high-risk group was significantly worse. ROC analysis showed that this risk score was very accurate in predicting OS at 1, 3, and 5 years in the TCGA READ cohort. Therefore, we selected another RC cohort from GEO for external validation. The results showed that there was still a significant difference in OS between the two groups. The accuracy of OS prediction, though decreased, was still above 0.6, indicating that the risk score has reasonable extrapolation ability. We briefly

checked the expression of the 14 genes encoded proteins through the HPA database, and found that only ATM was significantly highly expressed in RC tissue. Then, we performed qRT-PCR analysis of these 14 genes with surgical specimens from our research center, and the results showed that TP63, ISCU, PLIN4, MAP3K5, OXSR, FANCD2 and ATM were significantly highly expressed in tumor tissue. The reasons for the different results of IHC and qRT-PCR include: the sensitivity of IHC is not high, resulting in the failure to identify proteins with significant differences; there are some additional intervening factors in the process from transcription to translation, which need to be further explored.

We briefly introduce these 14 genes one by one. TP63 encodes a member of the p53 transcription factor family,



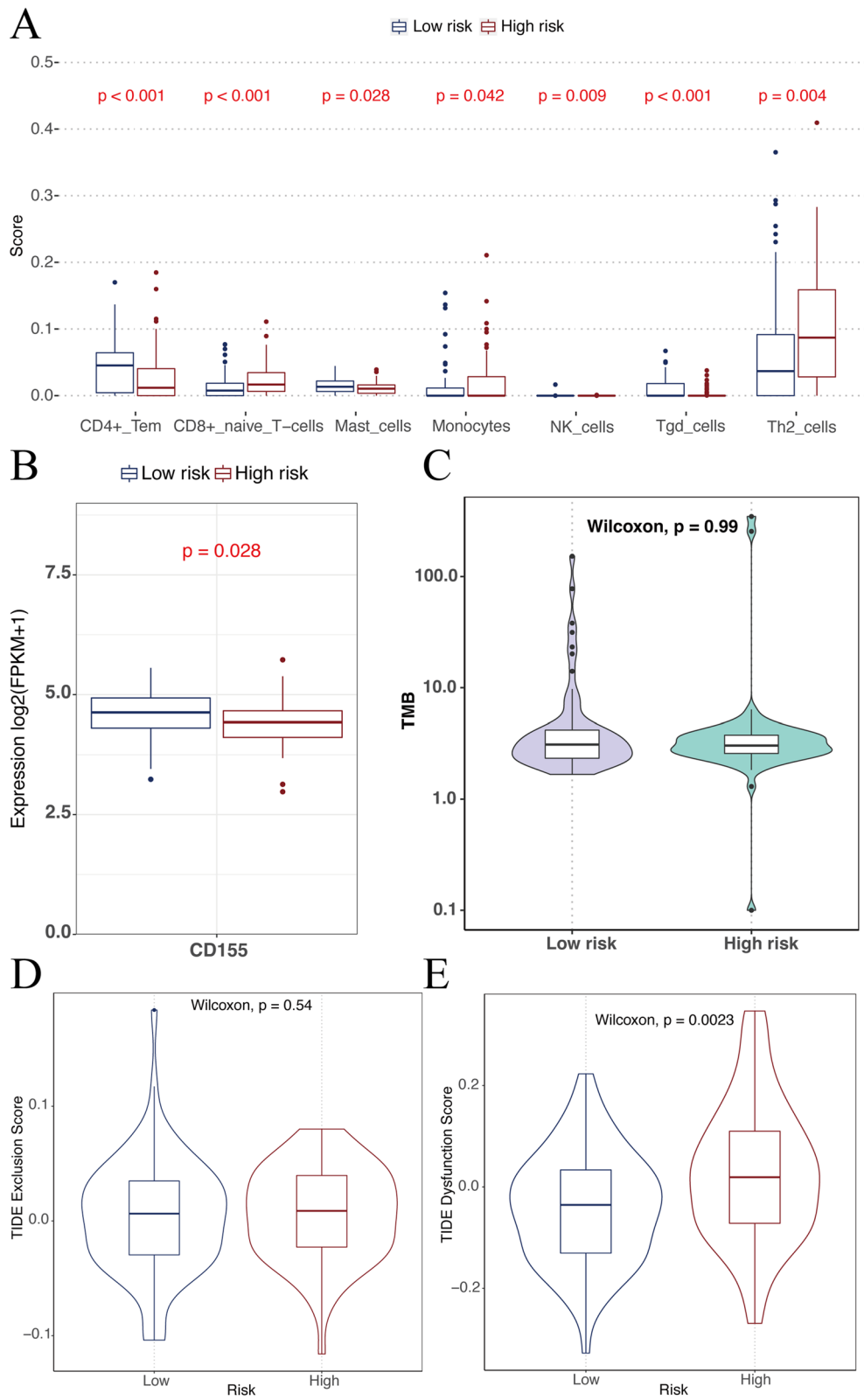
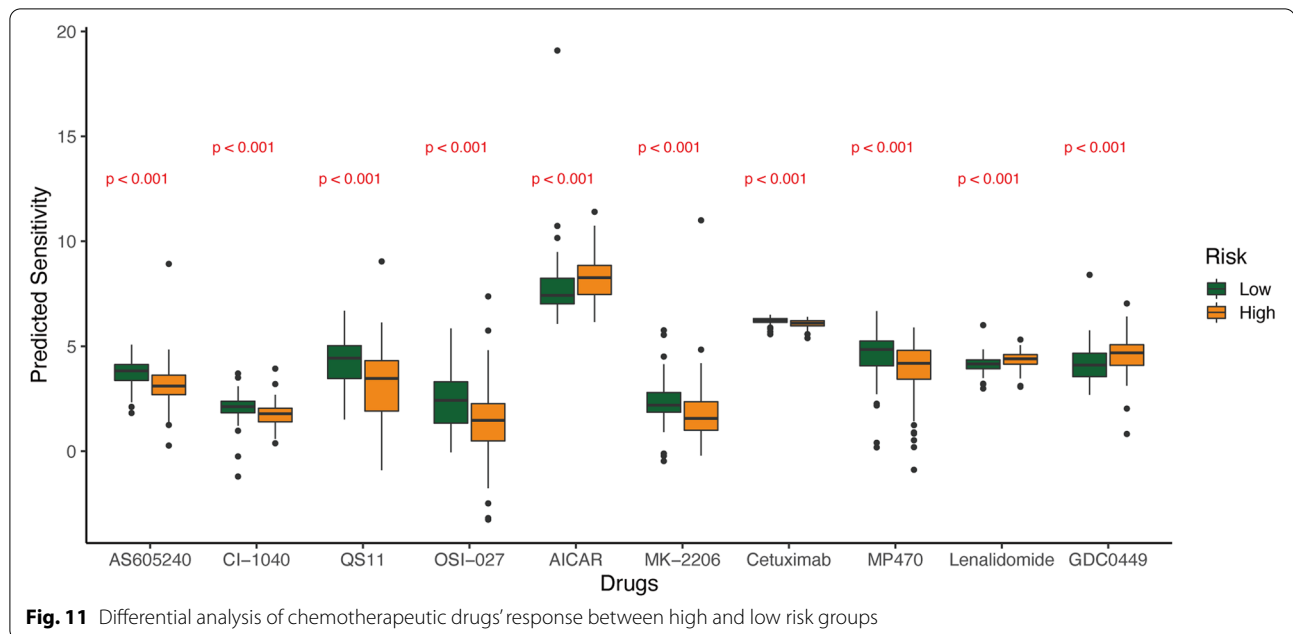


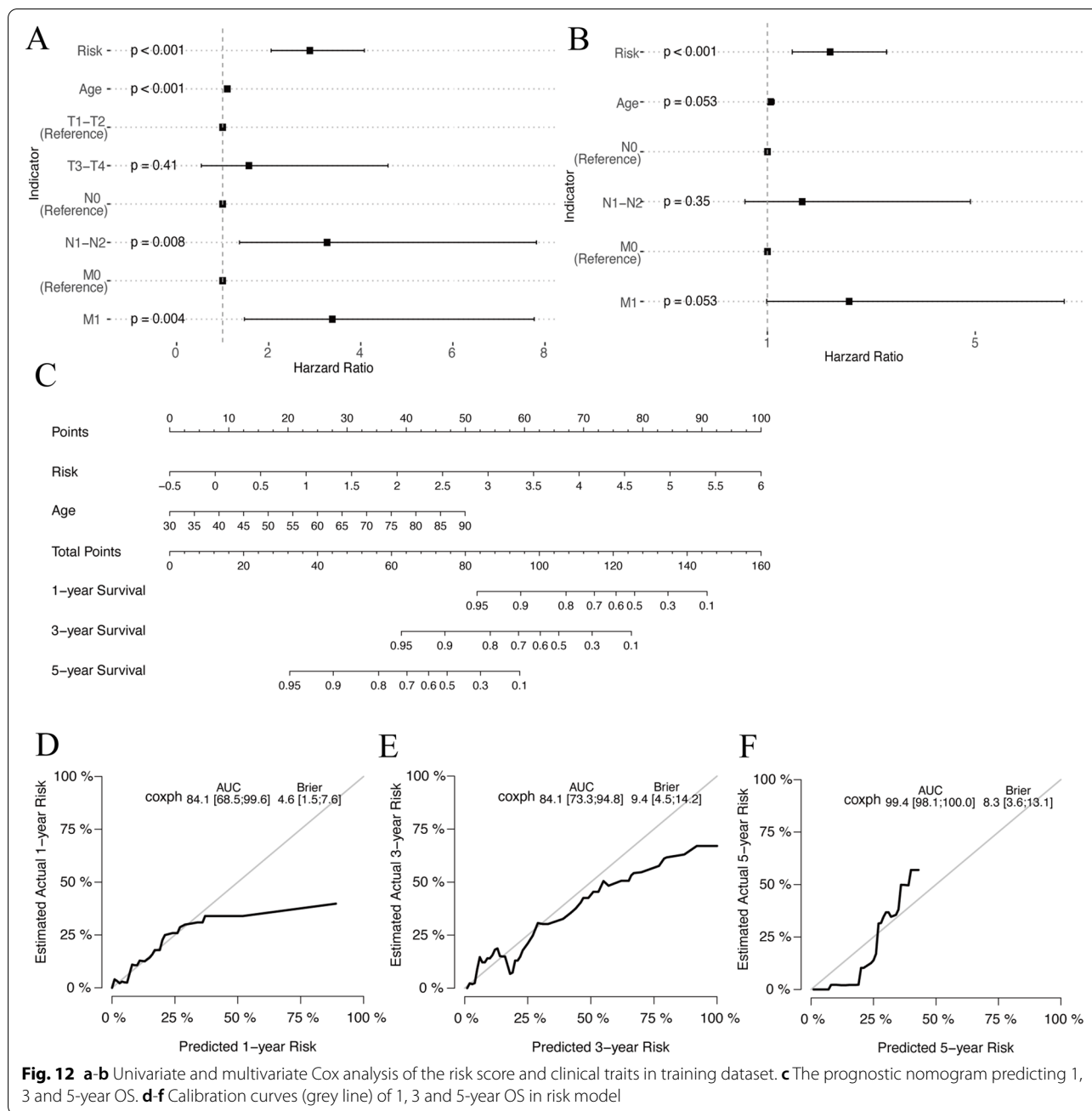
Fig. 10 **a** Difference of immune cells' scores between high- and low-risk groups. **b** Differential analysis of immune checkpoint expression between two groups. **c** Difference of TMB between two groups. **d-e** Difference of TIDE scores between two groups



and studies have shown that up-regulation of TP63 may further activate the glutathione metabolic pathways, including GPX4, thus reducing cellular exposure to oxidative stress, which supports the survival of tumor cells [33, 34]. ISCU encodes a component of the iron-sulfur (Fe-S) cluster scaffold. As an important redox center, iron-sulfur clusters have participated in numerous physiological functions, particularly in the metabolism [35]. HSPB1 encodes a member of the small heat shock protein (HSP27), and its expression has been demonstrated to inhibit the ferroptosis process of tumor cells, thereby promoting tumor growth [36]. PLIN4 is linked to the formation of lipid droplets which store intracellular free fatty acids and inhibit lipotoxic cell death. Studies have shown that PLIN4 upregulation can increase the viability and drug resistance of tumor cells [37], and this process is likely to be closely related to the inhibition of ferroptosis. MAPK1, MAP3K5 and MAPK9 belong to MAPK-signaling systems which play major roles in tumors. They provide a connection between transmembrane signaling and changes in transcription in response to different environmental signals such as cytokines, growth factors, oxidative stress and inflammation [38]. Ferroptosis of certain sensitive cell lines may be blocked by MAPK inhibition [18]. Tumors with sustained MAPK activation are capable of responding to in vivo cystine depletion by inducing ferroptosis [39]. ABCC1 encodes multidrug resistance-associated protein 1 (MRP1) is a member of the superfamily of ATP-binding cassette (ABC) transporters. Studies have shown that cells overexpressing MRP1 can disrupt GSH homeostasis and hinder GPX4

activity, thereby making cells more susceptible to ferroptosis [40]. OXSR1 encodes a serine–threonine protein kinase, and studies have shown that high OSR1 expression causes an increase in deaths specifically attributed to breast cancer and is related to an increase in lymph node metastasis [41]. However, the specific mechanism remains to be explored. PANX1 encodes an ATP-releasing pathway family protein and PANX1 deletion protects against renal ischemia/reperfusion injury by attenuating the MAPK/ERK activation in a ferroptotic pathway [42]. FANCD2 encodes a nuclear protein involved in DNA damage repair. Studies have shown that it can protect against ferroptosis-mediated injury in bone marrow stromal cells [43]. In addition, it is significantly overexpressed in lung cancer tissue and is associated with the prognosis of lung cancer [44]. ATM encodes an important cell cycle checkpoint kinase. ATM inhibition rescued ferroptosis by increasing the expression of iron regulators involved in the storage and export of iron [45]. TUBE1 encodes a tubulin superfamily member that was included in a ferroptosis prognostic model of skin cutaneous melanoma [46]. ATG7 encodes an activation enzyme that is essential for autophagy and cytoplasmic to vacuole transport [47]. Knockdown of ATG7 may limit erastin-induced ferroptosis with decreased intracellular ferrous iron levels, and lipid peroxidation [48]. In conclusion, most of these 14 genes in the signature are closely related to ferroptosis and play an important role in tumor development, which merits further study.

We further analyzed the underlying mechanisms of different prognosis between high- and low-risk groups. The



GSEA results indicate that the enrichment pathways of the two groups are different. The high-risk group tends to be enriched in energy metabolism such as ribosomes, oxidative phosphorylation, and arachidonic acid metabolism. High-risk patients are likely to require the joint participation of the above pathways due to the inhibition of ferroptosis. Analysis of both groups of immune micro-environments found that, from the perspective of the ESTIMATE algorithm, the risk score was not correlated with the total number of immune cells and stromal cells.

However, there are significant differences in the number of different types of immune cells in high- and low-risk groups from the perspective of the xCELL algorithm, and the high-risk group has significantly more CD8+ naive T cells and Th2 cells. In CRC, a substantial density of CD8+ T-cells in tumor tissue is generally associated with a favorable prognosis and sensitivity to chemoradiotherapy and immunotherapy [49, 50], partly because CD8+ T cells enhance ferroptosis-specific lipid peroxidation in tumor cells and thereby improve the anti-tumor effect

of ferroptosis [51]. CD8⁺ naive T cells in the high-risk group were notably overexpressed, and further research may be required to explore the evolution process from naive to maturity. The TMB of the high- and low-risk groups was basically the same, which just showed that the ferroptosis risk score in this study was independent of the TMB level, and RC patients were grouped from a distinct perspective. Regarding the TIDE score, the dysfunction score was significantly greater in the high-risk group. The TIDE score is primarily used to measure tumor immune escape from tumor immune dysfunction. In clinical practice, a higher TIDE score was associated with poorer immune checkpoint blocking treatment and shorter survival [29]. This result shows that the immune dysfunction in the high-risk group is more serious, indirectly suggesting that there is a relationship between ferroptosis and the immune microenvironment, which needs to be further explored. Analysis of 34 immune checkpoints showed significantly lower expression of CD155 in the high-risk group, while no significant differences were found for the remaining checkpoints. CD155 gene is overexpressed, which begins at an early stage in tumorigenesis and continues to late stages in colorectal carcinoma [52]. Besides, CD155 interacts with TIGIT on natural killer cells and T cells may transmit inhibitory signals to immune cells [53]. The significantly lower expression of CD155 in the high-risk group suggests that this group of patients may have characteristics of insensitivity to immunotherapy.

Combined with the analysis of drug susceptibility in the database, it was suggested that patients in the high-risk group were more sensitive to certain drugs. Although the difference in IC₅₀ was not too large, it still provided us with an idea that these drugs may inhibit RC by enhancing ferroptosis. AS605240 is a kind of phosphatidylinositol 3-kinase (PI3K) gamma inhibitor. Studies have shown that oral administration of AS605240 in a mouse colitis model can reduce intestinal inflammation in mice through a number of immunomodulatory effects [54]. MK-2206 is an inhibitor of Akt in the PI3K/Akt/mTOR pathway, and a multicenter phase II clinical study has demonstrated that its combination with neoadjuvant therapy can improve the pathological complete response (pCR) rate of HR-negative and HER2-positive breast cancer [55]. OSI-027 is an inhibitor of mTOR downstream of PI3K and can inhibit colon cancer cell growth through the 4 EBP1/eIF 4 E/PUMA pathway [56]. At present, studies have found that activation of the PI3K/Akt/mTOR signaling pathway can inhibit the ferroptosis of tumor cells through lipid production [57]. It has been reported that PI3K inhibitors can induce immunogenic ferroptosis in

tumor cells, thereby achieving anticancer effects [32]. Therefore, PI3K pathway inhibitors induce ferroptosis by affecting the tumor immune microenvironment, and have broad research prospects in the field of colorectal cancer treatment. CI-1040 is a kind of MAPK inhibitor. An early multicenter phase II clinical study to explore oral CI-1040 in the treatment of multiple cancer types showed unsatisfactory results [58], so this medicine is basically eliminated. MP470 is a kind of receptor tyrosine kinase inhibitor, now known as amuvatinib [59]. It was used in a phase II clinical study of platinum-refractory small cell lung cancer patients, and the efficacy was not satisfactory [60]. QS11 is a kind of small molecule synergist with Wnt-3a ligand in the activation of Wnt/beta-catenin signal transduction [61]. A recent study on gastric cancer found that activation of the Wnt/beta-catenin signaling attenuates cellular lipid ROS production and subsequently inhibits ferroptosis [62]. Therefore, from the perspective of ferroptosis, QS11 may have the opposite effect. Studies have shown that the combined treatment of β -elemene and cetuximab is sensitive to KRAS mutant CRC cells by inducing ferroptosis, which will hopefully provide a prospective strategy for CRC patients with RAS mutations [63].

To further improve the clinical predictive value of the risk score, we combined common clinical prognostic factors (age and TNM stage) to construct a final prognostic model, which is composed of the risk score and age. 1-year, 3-year and 5-year OS were predicted, and the prediction accuracy was further improved compared with the risk score alone. We look forward to further discussion and promotion of the detailed mechanism of this model. In recent years, many clinical prognostic models have been built, involving various cancers and mechanisms [21, 64–66]. While the model presented in this study is still in its theoretical exploration stage, we hope that through this limited research it will provide a reference for more in-depth research on the mechanism of ferroptosis in the RC field in the future. There are also some obvious limitations in this study. Our cluster and DEGs analysis and subsequent risk model construction are two relatively independent parts. The former attempts to present different ferroptosis patterns in RC but is not discussed in detail. The latter is the main body of the article, which may confuse readers about the structure of this article. The data set selected for the bioinformatic analysis is itself a very small subset of RC patients. This subset inherently suffers from limited extrapolation, although we obtained acceptable results with the validation set. The sample size included in qRT-PCR is limited. If the sample size increases, the expression level of its mRNA may change on this basis.

Conclusions

This study provides a risk score of FRGs for RC by analyzing the TCGA READ cohort from the perspective of FRDs, which can effectively distinguish the prognosis of two groups of patients and predict 1-year, 3-year and 5-year OS. The 14 genes involved in this risk score may affect the occurrence and development of RC. It may also affect drug sensitivity from ferroptosis, immune infiltration and other aspects, providing a reference for further in-depth discussion. We constructed a more complete prognostic model combined with the clinical characteristics of the patients, which enhanced the predictive ability of the risk score.

Abbreviations

CRC: Colorectal Cancer; RC: Rectal Cancer; TME: Total Mesorectal Excision; nCRT: neoadjuvant Chemoradiotherapy; ctDNA: Circulating Tumor DNA; ICI: Immune Checkpoint Inhibitor; FRG: Ferroptosis-Related Gene; TCGA: The Cancer Genome Atlas; READ: Rectum Adenocarcinoma; GEO: Gene Expression Omnibus; HPA: Human Protein Atlas; IHC: Immunohistochemistry; DEG: Differentially Expressed Gene; t-SNE: t-distributed Stochastic Neighbor Embedding; FRDEG: Ferroptosis-related Differentially Expressed Gene; GO: Gene Ontology; KEGG: Kyoto Encyclopedia of Genes and Genomes; BP: Biological Process; CC: Cellular Composition; MF: Molecular Function; LASSO: Least Absolute Shrinkage and Selection Operator; K-M: Kaplan-Meier; ROC: Receiver Operating Characteristic; qRT-PCR: Quantitative Real-Time Polymerase Chain Reaction; GSEA: Gene Set Enrichment Analysis; MSigDB: Molecular Signatures Database; TMB: Tumor Mutation Burden; TIDE: Tumour Immune Dysfunction and Exclusion; OS: Overall Survival; BH: Benjaminiand Hochberg; GPX4: Glutathione Peroxidase 4; HR: Hazard Ratio; AUC: Area Under Curve; Fe-S: Iron-sulfur; MRP1: Multidrug Resistance-associated Protein 1; ABC: ATP-binding Cassette; PI3K: Phosphatidylinositol 3-Kinase; pCR: pathological Complete Response.

Supplementary Information

The online version contains supplementary material available at <https://doi.org/10.1186/s12864-022-08996-6>.

Additional file 1: Fig. S1. (A) Consensus matrix legend of the cluster. (B-I) The heatmap of consensus matrix with k from 2 to 9. (J) Consensus cumulative distribution function (CDF). (K) Relative change in area under CDF curve. (L) Tracking plot of the cluster.

Acknowledgements

The authors would like to express our sincere thanks for sharing the data from public database mentioned in this study.

Authors' contributions

WK Shi and GL Lin were responsible for the conception and design of the study. WK Shi performed the data analysis, experiment and wrote the manuscript. YX Liu, XY Qiu, JY Zhou and JL Zhou reviewed and revised the manuscript. All the authors read and approved the final manuscript.

Funding

This study was supported by Beijing Major Science and Technology Projects (D171100002617003).

Availability of data and materials

The datasets generated and analysed during the current study are available in the TCGA repository, <https://tcga-data.nci.nih.gov/tcga>. The independent validation cohort data is available in the GEO repository, <https://www.ncbi.nlm.nih.gov/geo> (GSE87211).

Declarations

Ethics approval and consent to participate

This study was approved by the Ethical Committee of Peking Union Medical Hospital (ethics number: I-22PJ069). All patients provided written informed consent. All methods were performed in accordance with the relevant guide lines and regulations.

Consent for publication

Not applicable.

Competing interests

The authors confirm that they have no competing interests.

Author details

¹Department of General Surgery, Peking Union Medical College Hospital, Peking Union Medical College and Chinese Academy of Medical Sciences, Shuaifuyuan 1, Beijing 100730, China. ²Department of Medical Records, Peking Union Medical College Hospital, Chinese Academy of Medical Sciences and Peking Union Medical College, Beijing, China. ³Collaborating Center for the WHO Family of International Classifications in China, Beijing, China.

Received: 21 June 2022 Accepted: 7 November 2022

Published online: 22 November 2022

References

1. Siegel RL, Miller KD, Fuchs HE, Jemal A. Cancer statistics, 2022. *CA Cancer J Clin.* 2022;72(1):7–33.
2. Sung H, Ferlay J, Siegel RL, Laversanne M, Soerjomataram I, Jemal A, et al. Global cancer statistics 2020: GLOBOCAN estimates of incidence and mortality worldwide for 36 cancers in 185 countries. *CA Cancer J Clin.* 2021.
3. Choi Y, Sateia HF, Peairs KS, Stewart RW. Screening for colorectal cancer. *Semin Oncol.* 2017;44(1):34–44.
4. Bipat S, Glas AS, Slors FJ, Zwinderman AH, Bossuyt PM, Stoker J. Rectal cancer: local staging and assessment of lymph node involvement with endoluminal US, CT, and MR imaging—a meta-analysis. *Radiology.* 2004;232(3):773–83.
5. Bach SP, Gilbert A, Brock K, Korsgen S, Geh I, Hill J, et al. Radical surgery versus organ preservation via short-course radiotherapy followed by transanal endoscopic microsurgery for early-stage rectal cancer (TREC): a randomised, open-label feasibility study. *Lancet Gastroenterol Hepatol.* 2021;6(2):92–105.
6. Sauer R, Liersch T, Merkel S, Fietkau R, Hohenberger W, Hess C, et al. Preoperative versus postoperative chemoradiotherapy for locally advanced rectal cancer: results of the German CAO/ARO/AIO-94 randomized phase III trial after a median follow-up of 11 years. *J Clin Oncol.* 2012;30(16):1926–33.
7. Bossset JF, Calais G, Mineur L, Maingon P, Stojanovic-Rundic S, Bensadoun RJ, et al. Fluorouracil-based adjuvant chemotherapy after preoperative chemoradiotherapy in rectal cancer: long-term results of the EORTC 22921 randomised study. *Lancet Oncol.* 2014;15(2):184–90.
8. Zhou J, Wang C, Lin G, Xiao Y, Jia W, Xiao G, et al. Serial circulating tumor DNA in predicting and monitoring the effect of neoadjuvant Chemoradiotherapy in patients with rectal Cancer: a prospective multicenter study. *Clin Cancer Res.* 2021;27(1):301–10.
9. Zhu J, Liu A, Sun X, Liu L, Zhu Y, Zhang T, et al. Multicenter, randomized, phase III trial of neoadjuvant Chemoradiation with Capecitabine and irinotecan guided by UGT1A1 status in patients with locally advanced rectal Cancer. *J Clin Oncol.* 2020;38(36):4231–9.
10. Tarpgaard LS, Andersen PV, Øgaard N, Demuth C, Andersen CL, Pfeiffer P. Complete pathological and serological response to immunotherapy in a patient with MMR-deficient early rectal cancer. *Ann Oncol.* 2021;32(6):805–6.
11. Dixon SJ, Lemberg KM, Lamprecht MR, Skouta R, Zaitsev EM, Gleason CE, et al. Ferroptosis: an iron-dependent form of nonapoptotic cell death. *Cell.* 2012;149(5):1060–72.

12. Jiang X, Stockwell BR, Conrad M. Ferroptosis: mechanisms, biology and role in disease. *Nat Rev Mol Cell Biol.* 2021;22(4):266–82.
13. Lu Y, Qin H, Jiang B, Lu W, Hao J, Cao W, et al. KLF2 inhibits cancer cell migration and invasion by regulating ferroptosis through GPX4 in clear cell renal cell carcinoma. *Cancer Lett.* 2021;522:1–13.
14. Kuang F, Liu J, Xie Y, Tang D, Kang R. MGS1 is a redox-sensitive repressor of ferroptosis in pancreatic cancer cells. *Cell Chem Biol.* 2021;28(6):765–775.e765.
15. Yadav P, Sharma P, Sundaram S, Venkatraman G, Bera AK, Karunakaran D. SLC7A11/xCT is a target of miR-5096 and its restoration partially rescues miR-5096-mediated ferroptosis and anti-tumor effects in human breast cancer cells. *Cancer Lett.* 2021;522:211–24.
16. Zhou N, Bao J. FerrDb: a manually curated resource for regulators and markers of ferroptosis and ferroptosis-disease associations. *Database (Oxford).* 2020;2020.
17. Dixon SJ, Patel DN, Welsch M, Skouta R, Lee ED, Hayano M, et al. Pharmacological inhibition of cystine–glutamate exchange induces endoplasmic reticulum stress and ferroptosis. *Elife.* 2014;3:e02523.
18. Yagoda N, von Rechenberg M, Zaganjor E, Bauer AJ, Yang WS, Fridman DJ, et al. RAS-RAF-MEK-dependent oxidative cell death involving voltage-dependent anion channels. *Nature.* 2007;447(7146):864–8.
19. Wang L, Liu Y, Du T, Yang H, Lei L, Guo M, et al. ATF3 promotes erastin-induced ferroptosis by suppressing system xc0. *Cell Death Differ.* 2020;27(2):662–75.
20. Chen L, Qiao L, Bian Y, Sun X. GDF15 knockdown promotes erastin-induced ferroptosis by decreasing SLC7A11 expression. *Biochem Biophys Res Commun.* 2020;526(2):293–9.
21. Shao Y, Jia H, Huang L, Li S, Wang C, Aikemu B, et al. An original Ferroptosis-related gene signature effectively predicts the prognosis and clinical status for colorectal Cancer patients. *Front Oncol.* 2021;11:711776.
22. Hong Z, Tang P, Liu B, Ran C, Yuan C, Zhang Y, et al. Ferroptosis-related genes for overall survival prediction in patients with colorectal Cancer can be inhibited by Gallic acid. *Int J Biol Sci.* 2021;17(4):942–56.
23. Wilkerson MD, Hayes DN. ConsensusClusterPlus: a class discovery tool with confidence assessments and item tracking. *Bioinformatics.* 2010;26(12):1572–3.
24. van der Maaten L, Hinton G. Visualizing Data using t-SNE. *J Mach Learn Res.* 2008;9:2579–605.
25. Ritchie ME, Phipson B, Wu D, Hu Y, Law CW, Shi W, et al. Limma powers differential expression analyses for RNA-sequencing and microarray studies. *Nucleic Acids Res.* 2015;43(7):e47.
26. Yu G, Wang LG, Han Y, He QY. clusterProfiler: an R package for comparing biological themes among gene clusters. *OMICS.* 2012;16(5):284–7.
27. Kanehisa M, Goto S. KEGG: Kyoto encyclopedia of genes and genomes. *Nucleic Acids Res.* 2000;28(1):27–30.
28. Aran D, Hu Z, Butte AJ. xCell: digitally portraying the tissue cellular heterogeneity landscape. *Genome Biol.* 2017;18(1):220.
29. Jiang P, Gu S, Pan D, Fu J, Sahu A, Hu X, et al. Signatures of T cell dysfunction and exclusion predict cancer immunotherapy response. *Nat Med.* 2018;24(10):1550–8.
30. Geleher P, Cox N, Huang RS. pRRophetic: an R package for prediction of clinical chemotherapeutic response from tumor gene expression levels. *PLoS One.* 2014;9(9):e107468.
31. Friedmann Angeli JP, Krysko DV, Conrad M. Ferroptosis at the crossroads of cancer-acquired drug resistance and immune evasion. *Nat Rev Cancer.* 2019;19(7):405–14.
32. Fan F, Liu P, Bao R, Chen J, Zhou M, Mo Z, et al. A dual PI3K/HDAC inhibitor induces immunogenic Ferroptosis to potentiate Cancer immune checkpoint therapy. *Cancer Res.* 2021;81(24):6233–45.
33. Wang GX, Tu HC, Dong Y, Skanderup AJ, Wang Y, Takeda S, et al. ΔNp63 inhibits oxidative stress-induced cell death, including Ferroptosis, and cooperates with the BCL-2 family to promote Clonogenic survival. *Cell Rep.* 2017;21(10):2926–39.
34. Wang Y, Zhao G, Condello S, Huang H, Cardenas H, Tanner EJ, et al. Frizzled-7 identifies platinum-tolerant ovarian Cancer cells susceptible to Ferroptosis. *Cancer Res.* 2021;81(2):384–99.
35. Xu XM, Möller SG. Iron-sulfur clusters: biogenesis, molecular mechanisms, and their functional significance. *Antioxid Redox Signal.* 2011;15(1):271–307.
36. Sun X, Ou Z, Xie M, Kang R, Fan Y, Niu X, et al. HSPB1 as a novel regulator of ferroptotic cancer cell death. *Oncogene.* 2015;34(45):5617–25.
37. Sirois I, Aguilar-Mahecha A, Laffleur J, Fowler E, Vu V, Scriver M, et al. A unique morphological phenotype in Chemoresistant triple-negative breast Cancer reveals metabolic reprogramming and PLIN4 expression as a molecular vulnerability. *Mol Cancer Res.* 2019;17(12):2492–507.
38. Slattery ML, Lundgreen A, Wolff RK. MAP kinase genes and colon and rectal cancer. *Carcinogenesis.* 2012;33(12):2398–408.
39. Poursaitidis I, Wang X, Crighton T, Labuschagne C, Mason D, Cramer SL, et al. Oncogene-selective sensitivity to nutrient Cystine. *Cell Rep.* 2017;18(11):2547–56.
40. Hanssen KM, Haber M, Fletcher JI. Targeting multidrug resistance-associated protein 1 (MRP1)-expressing cancers: beyond pharmacological inhibition. *Drug Resist Updat.* 2021;59:100795.
41. Li Y, Qin J, Wu J, Dai X, Xu J. High expression of OSR1 as a predictive biomarker for poor prognosis and lymph node metastasis in breast cancer. *Breast Cancer Res Treat.* 2020;182(1):35–46.
42. Su L, Jiang X, Yang C, Zhang J, Chen B, Li Y, et al. Pannexin 1 mediates ferroptosis that contributes to renal ischemia/reperfusion injury. *J Biol Chem.* 2019;294(50):19395–404.
43. Song X, Xie Y, Kang R, Hou W, Sun X, Epperly MW, et al. FANCD2 protects against bone marrow injury from ferroptosis. *Biochem Biophys Res Commun.* 2016;480(3):443–9.
44. Miao H, Ren Q, Li H, Zeng M, Chen D, Xu C, et al. Comprehensive analysis of the autophagy-dependent ferroptosis-related gene FANCD2 in lung adenocarcinoma. *BMC Cancer.* 2022;22(1):225.
45. Chen PH, Wu J, Ding CC, Lin CC, Pan S, Bossa N, et al. Kinome screen of ferroptosis reveals a novel role of ATM in regulating iron metabolism. *Cell Death Differ.* 2020;27(3):1008–22.
46. Ping S, Wang S, Zhao Y, He J, Li G, Li D, et al. Identification and validation of a ferroptosis-related gene signature for predicting survival in skin cutaneous melanoma. *Cancer Med.* 2022.
47. Kessel DH, Price M, Reiners JJ Jr. ATG7 deficiency suppresses apoptosis and cell death induced by lysosomal photodamage. *Autophagy.* 2012;8(9):1333–41.
48. Hou W, Xie Y, Song X, Sun X, Lotze MT, Zeh HJ 3rd, et al. Autophagy promotes ferroptosis by degradation of ferritin. *Autophagy.* 2016;12(8):1425–8.
49. Farchouk L, Hartman DJ, Ma C, Celebrezze J, Medich D, Bahary N, et al. Intratumoral budding and automated CD8-positive T-cell density in pretreatment biopsies can predict response to neoadjuvant therapy in rectal adenocarcinoma. *Mod Pathol.* 2021;34(1):171–83.
50. Shang S, Yang YW, Chen F, Yu L, Shen SH, Li K, et al. TRIB3 reduces CD8(+) T cell infiltration and induces immune evasion by repressing the STAT1-CXCL10 axis in colorectal cancer. *Sci Transl Med.* 2022;14(626):eabf0992.
51. Wang W, Green M, Choi JE, Gijón M, Kennedy PD, Johnson JK, et al. CD8(+) T cells regulate tumour ferroptosis during cancer immunotherapy. *Nature.* 2019;569(7755):270–4.
52. Masson D, Jarry A, Baury B, Blanchardie P, Laboisie C, Lustenberger P, et al. Overexpression of the CD155 gene in human colorectal carcinoma. *Gut.* 2001;49(2):236–40.
53. Wang D, Gu Y, Yan X, Huo C, Wang G, Zhao Y, et al. Role of CD155/TIGIT in digestive cancers: promising Cancer target for immunotherapy. *Front Oncol.* 2022;12:844260.
54. Dutra RC, Cola M, Leite DF, Bento AF, Claudino RF, Nascimento AF, et al. Inhibitor of PI3K ameliorates TNBS-induced colitis in mice by affecting the functional activity of CD4+CD25+FoxP3+ regulatory T cells. *Br J Pharmacol.* 2011;163(2):358–74.
55. Chien AJ, Tripathy D, Albain KS, Symmans WF, Rugo HS, Melisko ME, et al. MK-2206 and standard neoadjuvant chemotherapy improves response in patients with human epidermal growth factor receptor 2-positive and/or hormone receptor-negative breast cancers in the I-SPY 2 trial. *J Clin Oncol.* 2020;38(10):1059–69.
56. Wang H, Liu Y, Ding J, Huang Y, Liu J, Liu N, et al. Targeting mTOR suppressed colon cancer growth through 4EBP1/eIF4E/PUMA pathway. *Cancer Gene Ther.* 2020;27(6):448–60.
57. Yi J, Zhu J, Wu J, Thompson CB, Jiang X. Oncogenic activation of PI3K-AKT-mTOR signaling suppresses ferroptosis via SREBP-mediated lipogenesis. *Proc Natl Acad Sci U S A.* 2020;117(49):31189–97.
58. Rinehart J, Adjei AA, Lorusso PM, Waterhouse D, Hecht JR, Natale RB, et al. Multicenter phase II study of the oral MEK inhibitor, CI-1040, in patients with advanced non-small-cell lung, breast, colon, and pancreatic cancer. *J Clin Oncol.* 2004;22(22):4456–62.

59. Zhao H, Luoto KR, Meng AX, Bristow RG. The receptor tyrosine kinase inhibitor amuvatinib (MP470) sensitizes tumor cells to radio- and chemotherapy in part by inhibiting homologous recombination. *Radiother Oncol.* 2011;101(1):59–65.
60. Byers LA, Horn L, Ghandi J, Kloecker G, Owonikoko T, Waqar SN, et al. A phase 2, open-label, multi-center study of amuvatinib in combination with platinum etoposide chemotherapy in platinum-refractory small cell lung cancer patients. *Oncotarget.* 2017;8(46):81441–54.
61. Zhang Q, Major MB, Takanashi S, Camp ND, Nishiya N, Peters EC, et al. Small-molecule synergist of the Wnt/beta-catenin signaling pathway. *Proc Natl Acad Sci U S A.* 2007;104(18):7444–8.
62. Wang Y, Zheng L, Shang W, Yang Z, Li T, Liu F, et al. Wnt/beta-catenin signaling confers ferroptosis resistance by targeting GPX4 in gastric cancer. *Cell Death Differ.* 2022.
63. Chen P, Li X, Zhang R, Liu S, Xiang Y, Zhang M, et al. Combinative treatment of β -elemene and cetuximab is sensitive to KRAS mutant colorectal cancer cells by inducing ferroptosis and inhibiting epithelial-mesenchymal transformation. *Theranostics.* 2020;10(11):5107–19.
64. Shi J, Wu P, Sheng L, Sun W, Zhang H. Ferroptosis-related gene signature predicts the prognosis of papillary thyroid carcinoma. *Cancer Cell Int.* 2021;21(1):669.
65. Tang X, Jiang F, Wang X, Xia Y, Mao Y, Chen Y. Identification of the Ferroptosis-related long non-coding RNAs signature to improve the prognosis prediction in papillary renal cell carcinoma. *Front Surg.* 2022;9:741726.
66. Chen X, Yan L, Jiang F, Lu Y, Zeng N, Yang S, et al. Identification of a Ferroptosis-related signature associated with prognosis and immune infiltration in adrenocortical carcinoma. *Int J Endocrinol.* 2021;2021:4654302.

Publisher's Note

Springer Nature remains neutral with regard to jurisdictional claims in published maps and institutional affiliations.

Ready to submit your research? Choose BMC and benefit from:

- fast, convenient online submission
- thorough peer review by experienced researchers in your field
- rapid publication on acceptance
- support for research data, including large and complex data types
- gold Open Access which fosters wider collaboration and increased citations
- maximum visibility for your research: over 100M website views per year

At BMC, research is always in progress.

Learn more biomedcentral.com/submissions

